IEEE Access
Multidisciplinary ⋮ Rapid Review ⋮ Open Access Journal

Received December 29, 2020, accepted January 16, 2021, date of publication January 19, 2021, date of current version January 26, 2021.

Digital Object Identifier 10.1109/ACCESS.2021.3052876

Lane-by-Lane Traffic Monitoring Using 24.1 GHz FMCW Radar System

HAE-SEUNG LIM[1], HYUNG-MIN PARK[1], (Senior Member, IEEE), JAE-EUN LEE[2], YONG-HWA KIM[3], (Member, IEEE), AND SEONGWOOK LEE[4], (Member, IEEE)

[1]Department of Electronic Engineering, Sogang University, Seoul 04107, Republic of Korea
[2]Bitsensing Inc., Seoul 04778, Republic of Korea
[3]Department of Electronic Engineering, Myongji University, Yongin 17058, Republic of Korea
[4]School of Electronics and Information Engineering, College of Engineering, Korea Aerospace University, Goyang 10540, Republic of Korea

Corresponding author: Seongwook Lee (swl90@kau.ac.kr)

This work was supported by the 2020 Korea Aerospace University Faculty Research Grant 2020-01-003.

ABSTRACT In this article, we propose a method to monitor traffic on the road using a 24.1 GHz radar system. In our work, we design our own traffic monitoring radar system from radar hardware, such as antenna systems and the transceiver, to radar software, such as detection and tracking algorithms. The radar we developed uses frequency-modulated continuous waveforms with a center frequency of 24.1 GHz, and its range resolution is tens of centimeters, which is enough to distinguish vehicles in multiple lanes. In addition, we can effectively distinguish vehicles by estimating their angles using an array antenna system. To evaluate the performance of our radar, we install it on the pedestrian overpass facing the road. From actual measurement results, our radar system can reliably estimate the distance to the vehicle, the speed of the vehicle, and the angle of the vehicle for a total of four lanes up to 300 m in real time. The traffic monitoring system using a radar sensor can compensate for the disadvantages of the camera-based road monitoring method.

INDEX TERMS Target detection and tracking, traffic monitoring, FMCW radar system.

I. INTRODUCTION

One of the prerequisites for building an intelligent transportation system is the measurement of road traffic. The most common sensor used to monitor traffic on the road is the vision sensor, such as a camera [1]. However, in the case of a camera sensor, its object detection performance is severely deteriorated in a lightless environment. In addition, when using a camera, there is a problem that the privacy of a driver or a passenger cannot be protected. Therefore, we propose a method of monitoring road traffic using a radar sensor. Recently, radar sensors have been widely used in various fields. For example, a radar sensor is mounted on a vehicle and used to detect targets [2] or recognize driving environments [3]. In addition, radar sensors are also used to monitor people indoors [4] and to locate people inside a vehicle [5]. In the case of radar sensors, the detection performance is independent of the presence or absence of light. In addition, it is very effective in protecting the privacy of people because object detection is performed using radio waves instead of taking pictures or videos. Moreover, because the basic role of the radar sensor is the estimation of the position and the speed of the object, it can also serve as a speedometer.

Recently, studies for monitoring a traffic environment using a radar have been actively conducted. For example, the global system for mobile communications (GSM)-based passive radar to monitor the road traffic was introduced in [6], [7]. They suggested that they could detect the speed of the vehicle using a GSM-based radar, but they did not consider estimating the distance to the target at all. In addition, some researchers presented rough detection results and suggested the feasibility of road surveillance using passive radar systems [8] or using a low-cost radar sensor operating in the microwave band [9]. In [10], the authors presented a method for estimating range, speed, and angle information of vehicles using a 35 GHz interferometric linear frequency-modulated continuous wave (FMCW) radar. Because the interferometer radar estimates target information using the phase of the signal received from the antenna, the process of extracting target information is more complicated than the FMCW radar that uses the frequency difference between transmitted and received signals. In addition, if the phase noise is added to the

The associate editor coordinating the review of this manuscript and approving it for publication was Emanuele Crisostomi.

received signal, the detection results can be inaccurate and the phase-error correction must be conducted. In the most recent study [11], a method for classifying lanes by clustering a number of measurement points generated by vehicles driving in each lane has been proposed. The authors in [11] used a frequency-shift keying (FSK) radar system, which is unable to detect stationary objects. If the traffic monitoring radar cannot detect stationary objects on the road, it can lead to a serious accident.

In this article, to monitor road traffic using a radar sensor, we design our own radar system from hardware to software. Among the various radar systems, we use a frequency-modulated continuous wave (FMCW) radar that uses a center frequency of 24.1 GHz. The 24 GHz band is one of the industrial, scientific, and medical (ISM) radio bands, which is a frequency band commonly used in automotive radar systems. Therefore, we design antenna systems and transceivers that can operate efficiently in this frequency band. In addition, the beamwidths of the transmit and receiving antennas are designed to cover four lanes up to 300 m on the highway. The FMCW radar has the advantage of high range resolution due to its high pulse compression ratio [12]. The range resolution of our radar waveform becomes tens of centimeters, so we can effectively distinguish vehicles in each lane.

Next, a radar signal processing algorithm is applied to the raw radar signal to extract targets' range, velocity, and angle information. When using the FMCW radar in which the frequency of a transmitted signal slowly increases and decreases with time, ambiguity may occur in estimating the range and velocity of the target [13]. Thus, to solve this range-velocity ambiguity problem, two types of up-chirp and down-chirp signals with the different time-frequency slopes are used. In addition, the array antenna is used as a receiving antenna for angle estimation. Using array signal processing, angle information of a target can be extracted from a phase difference between antenna elements. Finally, the target tracking is performed using the estimated position and velocity information of the target. After converting the estimated distance and angle information into two-dimensional (2D) distance information, the tracking algorithm using the probabilistic data association filter (PDAF) [14] is applied. When the PDAF is used, it is effective for tracking objects in linear motion.

To verify the performance of our traffic monitoring radar system, we mount our radar sensor on a pedestrian overpass and monitor actual road traffic. From actual measurement results, the radar system we designed can accurately estimate range, velocity, and angle information of targets and effectively track targets in four different lanes on the highway. In addition, our radar system can monitor road traffic in real time. Compared to the traffic monitoring radars suggested in [6], [7], [9], our radar can acquire all the distance, velocity, and angle information of the target simultaneously. Also, because it is not an interferometric radar in [10], it has the advantage of being resistant to the phase noise. In addition, unlike the FSK modulation in [11], our FMCW radar system can detect even stationary targets. In [15], [16], the author presented a tracking algorithm for a 24 GHz traffic monitoring FMCW radar. The methods in [15], [16] can operate effectively when the prior information, such as the road position, the lane orientation, and the surrounding road map, is known. However, the PDAF-based tracking we use does not require such prior information.

The remainder of this article is organized as follows. In Section II, we introduce our 24.1 GHz FMCW radar sensor for traffic monitoring. Then, the radar signal processing method for our radar system is explained in Section III. In particular, target detection and tracking algorithms using the radar sensor is covered in detail in this section. In Section IV, we analyze actual measurement results obtained by mounting a radar sensor on a pedestrian overpass. Finally, we conclude this article in Section V.

II. 24.1 GHz FMCW RADAR SENSOR FOR TRAFFIC MONITORING

In this section, we describe the structure of the radar hardware we designed. First, a series-fed patch array antenna was used as the antenna system (e.g., Tx and Rx) of the radar, which is shown in Fig. 1. This antenna system is a 1×4 single-input multiple-output (SIMO) antenna system consisting of 1 Tx and 4 Rxs. Each TX and RX consists of several columns of series-fed patches. In addition, the antenna spacing between the receiving antenna elements d is $\frac{3}{2}\lambda = \frac{3c}{2f_c}$, where f_c, λ, and c denote the center frequency of the radar waveform, the wavelength corresponding to the center frequency, and the propagation velocity of the radar signal. In general, the wider the antenna spacing, the better the angular resolution [17]. Even if the antenna spacing wider than $\frac{1}{2}\lambda$ results in a grating lobe, the antenna spacing was set as $\frac{3}{2}\lambda$ to obtain the angular resolution that the system targets. Here, we use the waveform with the center frequency of 24.1 GHz, and the values of f_c and λ become 24.1 GHz and 1.24 cm.

In addition, because we use 200 MHz bandwidth around 24.1 GHz in the FMCW radar, the antenna beam pattern from 24.0 GHz to 24.2 GHz is important. Fig. 2 shows the antenna

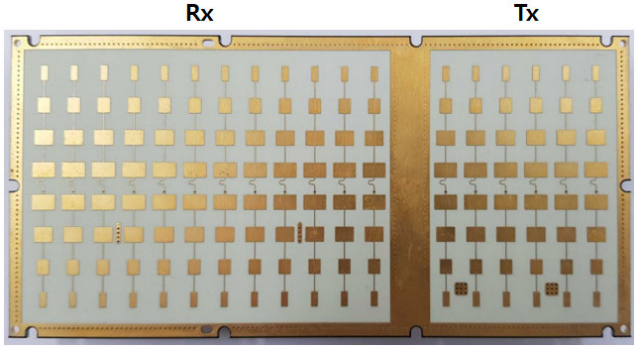

FIGURE 1. Antenna system of the 24.1 GHz FMCW radar sensor: 1×4 SIMO antenna system.

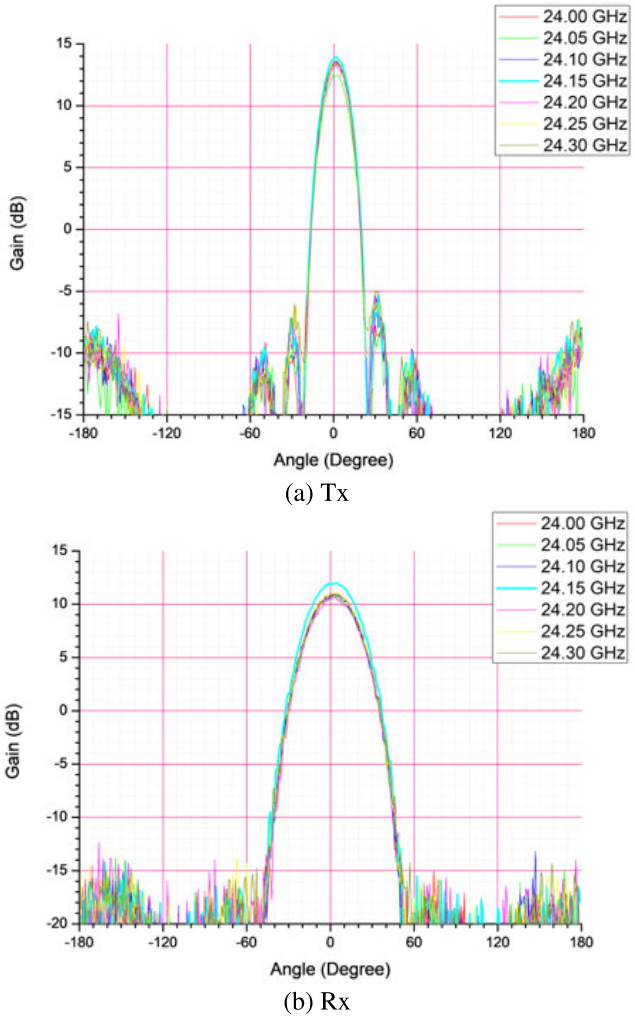

FIGURE 2. Antenna beam patterns in the azimuth direction: (a) the transmit antenna (b) and one receiving antenna element in the array antenna.

beam patterns of the transmit antenna and one receiving antenna element in the azimuth direction from 24.0 GHz to 24.3 GHz. As shown in this figure, the beam patterns are very stable in the selected frequency range. When we designed our antenna system, the Taylor line source method [18] was used to lower the sidelobe level (SSL). In addition, the ground (GND) via structure was applied to alleviate the coupling problem between the Tx and Rxs. This GND via is also used to prevent deterioration of the beam pattern due to surface waves. The parameter values related to the antenna system are given in Table 1. In this table, the antenna characteristics for one Tx element and one Rx element are presented.

The rear side of the antenna board (i.e., the front-end of the radar) is shown in Fig. 3, which consists of the power supply block, the analog-to-digital converter (ADC) block, and the radio frequency (RF) block. First, a signal with a center frequency of 24.1 GHz is generated from the phase-locked loop (PLL) and the voltage-controlled oscillator (VCO). This signal passes through the band-pass filter, and a transmitted

TABLE 1. Parameter values related to the antenna system.

Parameter	Value
Tx antenna gain (dB)	13.6
Tx SSL (dBc)	18.8
Tx 3 dB beamwidth (deg.)	18.56
Tx output power (dBm)	19.7
Rx antenna gain (dB)	10.8
Rx SSL (dBc)	23
Rx 3 dB beamwidth (deg.)	36.35
Rx return loss (dB)	-12.4

signal is generated therefrom. Then, the transmitted signal passes through a 2-way power divider and it becomes the inputs of the transmit antenna and the frequency mixers at the receiving end. At the receiving end, two chips capable of receiving in two radio channels are arranged to acquire a total of four channels of baseband radar signals. Then, the four baseband analog signals are converted to the digital signals through the ADC, and the converted digital signals are transferred to the back-end of the radar through the connector. Finally, the radar signal processing using the baseband signal is performed at the back-end of the radar.

Fig. 4 shows the back-end of our radar. We used Xilinx's Zynq 7020 as a computing unit to execute the radar signal processing we developed. The signal processing algorithms are performed on the ARM processor, and a field-programmable gate array (FPGA) is used to reduce computation time. Through the FPGA, radar pre-processing operation and multi-core processing are possible. In addition, the external interface is configured to enable the ethernet, RS-485, and WiFi. Our radar is also equipped with a camera, which is used to acquire images to evaluate radar detection results. Finally, Fig. 5 shows the size of the finished radar product we designed.

III. RADAR SIGNAL PROCESSING FOR TARGET DETECTION AND TRACKING

A. SIGNAL PROCESSING FOR TARGET DETECTION

We can acquire raw radar signals with the radar hardware designed in Section II. In this section, we describe how to estimate the distance to the target, the speed of the target, and the angle of the target from the received radar signal.

1) TARGET RANGE AND VELOCITY ESTIMATION

Fig. 6 shows a schematic block diagram for the radar signal processing, where the LPF and DSP represent the low-pass filter and the digital signal processor. In this FMCW radar system, the frequency of a transmitted signal increases and decreases linearly over time. The time-frequency slope of the transmitted FMCW radar signal in the first frame is shown in Fig. 7. As shown in Fig. 7, the transmitted signal can be divided into four signals according to time: $s_t^{(1)}(t)$ in $0 < t \leq \Delta T$, $s_t^{(2)}(t)$ in $\Delta T < t \leq 2\Delta T$, $s_t^{(3)}(t)$ in $2\Delta T < t \leq 4\Delta T$, and $s_t^{(4)}(t)$ in $4\Delta T < t \leq 6\Delta T$.

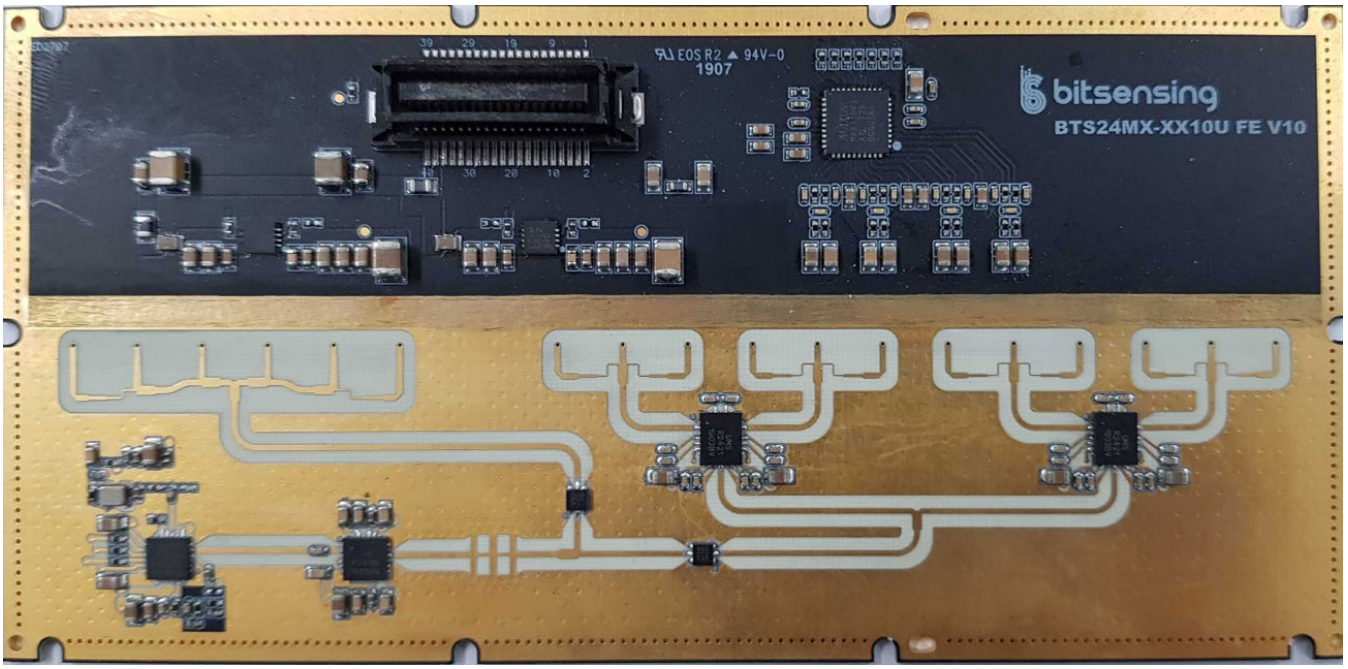

(a)

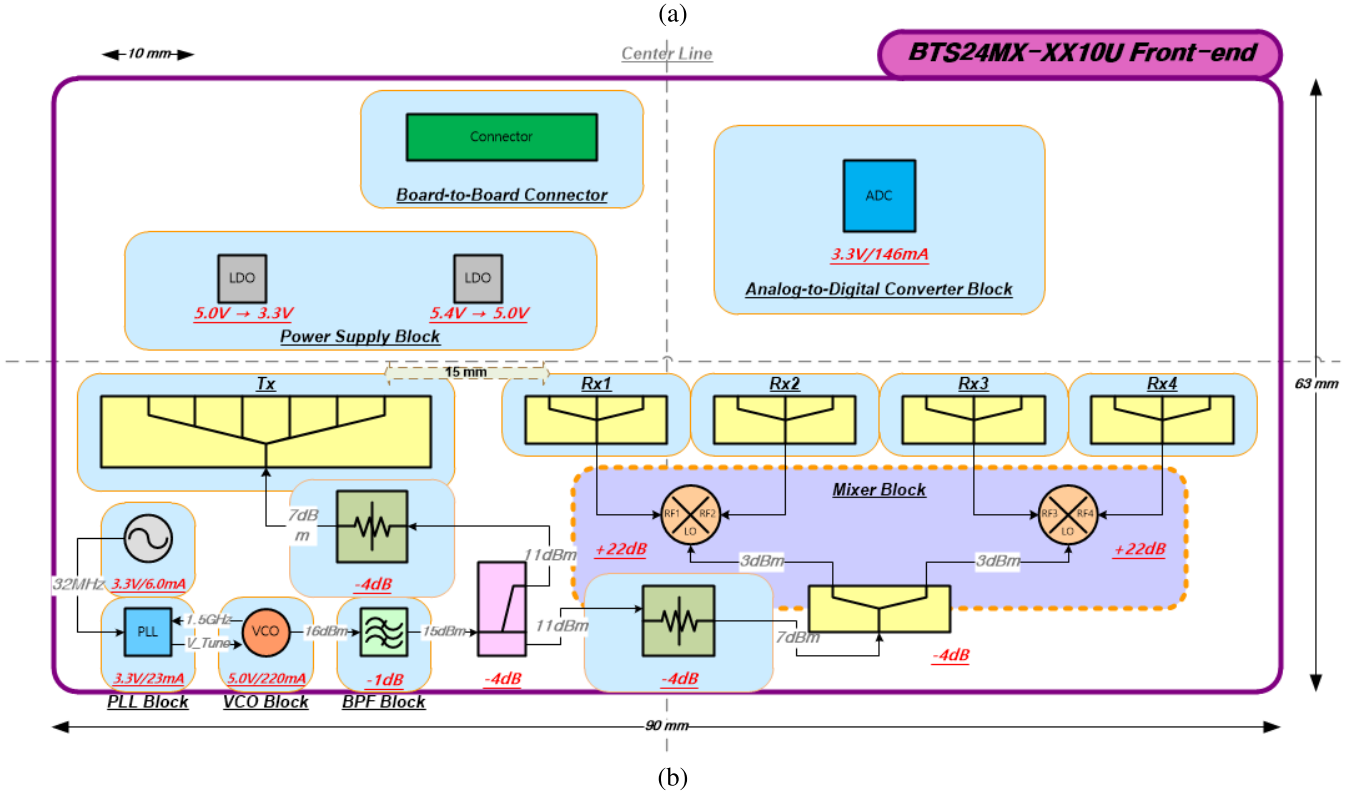

(b)

FIGURE 3. The front-end of the radar: (a) a photograph (b) and a schematic diagram.

First, the transmitted signal $s_t^{(1)}(t)$ in $0 < t \leq \Delta T$ is expressed as

$$s_t^{(1)}(t) = A_T \cos\left(2\pi(f_c - \frac{\Delta B}{2})t + \pi\frac{\Delta B}{\Delta T}t^2\right) \quad (0 \leq t \leq \Delta T), \quad (1)$$

where A_T, ΔB, and ΔT are the amplitude, the bandwidth, and the sweep time of the transmitted FMCW signal. As mentioned in Section II, we set the center frequency f_c and the bandwidth ΔB as 24.1 GHz and 200 MHz, respectively. In addition, the sweep time ΔT is set as 5 ms. This transmitted FMCW signal is also referred to as an up-chirp signal because its frequency increases rapidly.

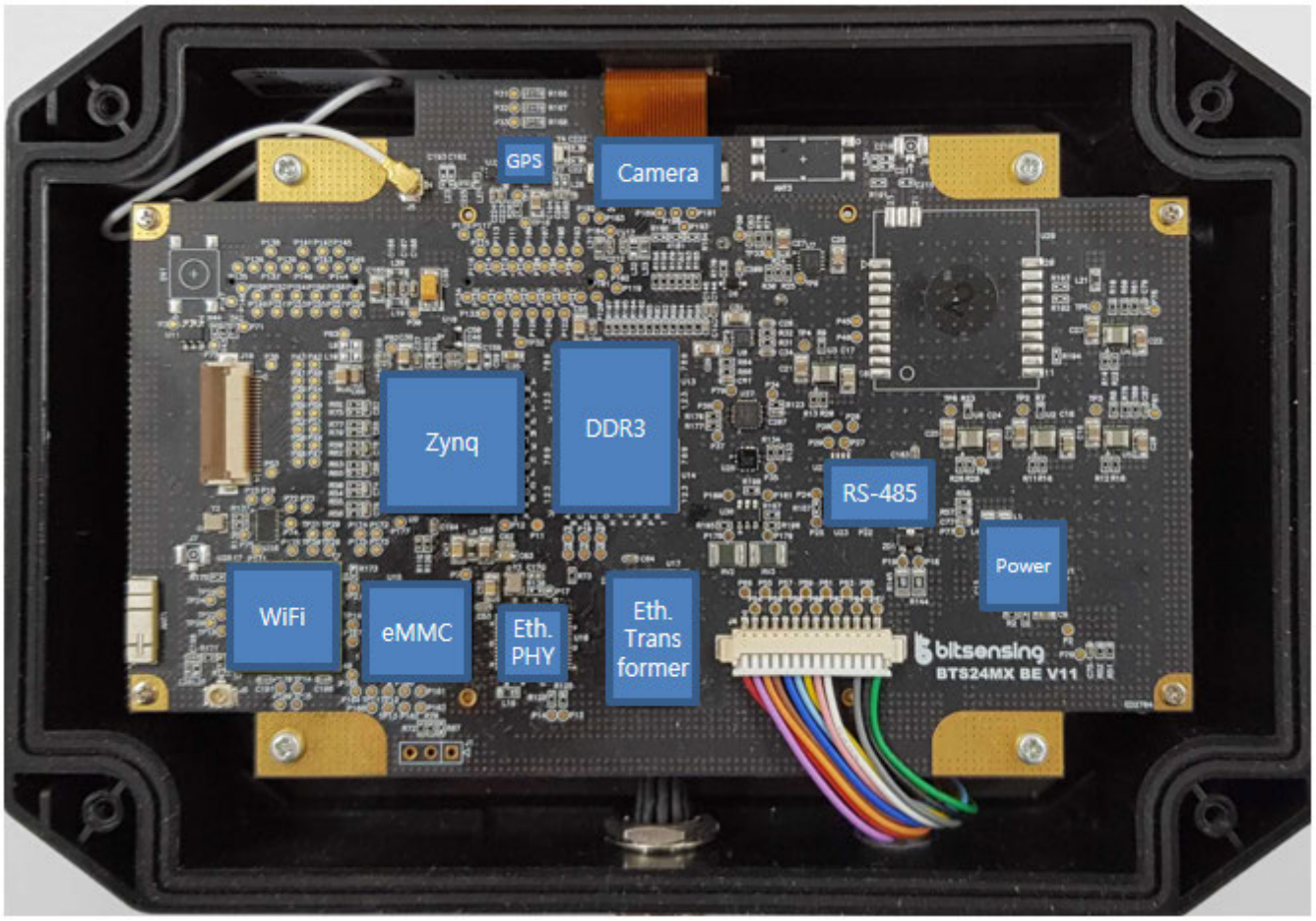

FIGURE 4. The back-end of the radar.

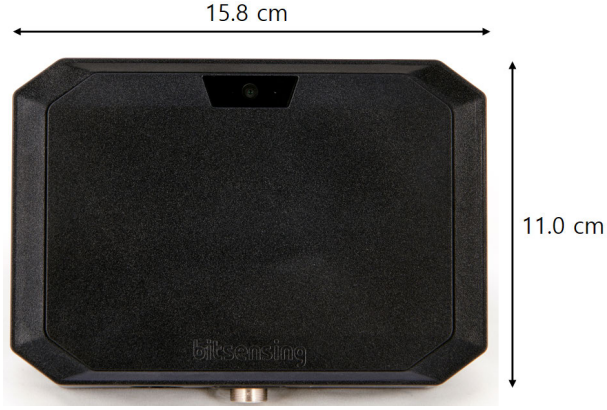

FIGURE 5. Size of our traffic monitoring radar.

When the transmitted FMCW signal is reflected from L targets, the received signal $s_r^{(1)}(t)$ can be expressed as

$$\begin{aligned} s_r^{(1)}(t) &= \sum_{l=1}^{L} \{A_{R_l} \cos(2\pi(f_c + f_{d_l} - \frac{\Delta B}{2})(t - t_{d_l}) \\ &\quad + \pi \frac{\Delta B}{\Delta T}(t - t_{d_l})^2)\} \\ &= \sum_{l=1}^{L} d_l(t), \end{aligned} \tag{2}$$

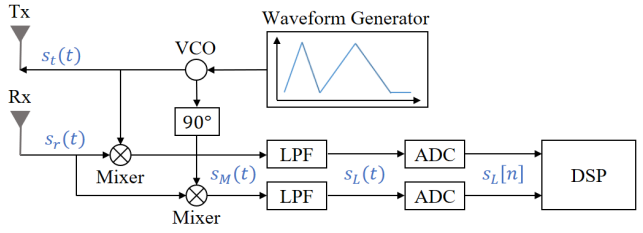

FIGURE 6. Schematic block diagram for radar signal processing.

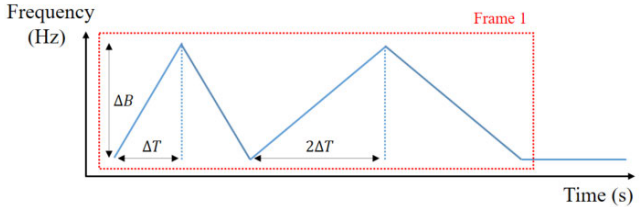

FIGURE 7. Time-frequency slope of the transmitted FMCW radar signal.

where A_{R_l} ($l = 1, 2, \cdots, L$) is the amplitude of the received signal reflected from the l_{th} target, f_{d_l} is the Doppler shift caused by the relative velocity between the l_{th} target and the radar, and t_{d_l} is the time delay caused by the relative distance between the l_{th} target and the radar. Here, we express the

desired received signal, which contains the range and the velocity information of the l_{th} target, as $d_l(t)$.

Then, the transmitted FMCW signal $s_t^{(1)}(t)$ is multiplied by the received radar signal $s_r^{(1)}(t)$ by passing through the frequency mixer. The output of the mixer $s_M^{(1)}(t)$ is given as

$$\begin{aligned} s_M^{(1)}(t) &= s_t^{(1)}(t)s_r^{(1)}(t) \\ &= s_t^{(1)}(t)\sum_{l=1}^{L} d_l(t). \end{aligned} \tag{3}$$

To extract the baseband signal from the frequency mixer output, $s_M^{(1)}(t)$ is passed through the LPF. Thus, the LPF output can be expressed as

$$\begin{aligned} s_L^{(1)}(t) = \frac{1}{2}A_T \sum_{l=1}^{L} A_{R_l} \cos(2\pi((\frac{\Delta B}{\Delta T}t_{d_l} - f_{d_l})t \\ + (f_c + f_{d_l} - \frac{\Delta B}{2})t_{d_l} - \frac{\Delta B}{2\Delta T}{t_{d_l}}^2)). \end{aligned} \tag{4}$$

Because the LPF output $s_L^{(1)}(t)$ consists of the sum of cosine waves, the frequency of each $d_l(t)$ can be extracted if we apply the Fourier transform. In practice, in the DSP in Fig. 6, a fast Fourier transform (FFT) is applied to the LPF output. At this time, the ordered statistic constant false alarm rate (OS-CFAR) algorithm [19] is applied to the LPF output to find the frequency in the noise components.

Then, the estimated frequency $\hat{f}_l^{(1)}$ of each $d_l(t)$ is expressed as

$$\begin{aligned} \hat{f}_l^{(1)} &= \frac{\Delta B}{\Delta T}t_{d_l} - f_{d_l} \\ &= \frac{\Delta B}{\Delta T}\frac{2R_l}{c} - \frac{2v_l}{c}f_c, \end{aligned} \tag{5}$$

where R_l and v_l are the relative distance and the relative velocity between the l_{th} target and the radar, respectively. This frequency is also called a beat frequency because it is the difference between the frequency of the transmitted radar signal and the frequency of the received radar signal.

Next, the transmitted signal $s_t^{(2)}(t)$ in $\Delta T < t \leq 2\Delta T$ can be expressed as

$$s_t^{(2)}(t) = A_T \cos\left(2\pi(f_c + \frac{3\Delta B}{2})t - \pi\frac{\Delta B}{\Delta T}t^2\right) \quad (\Delta T \leq t \leq 2\Delta T). \tag{6}$$

This transmitted signal is also referred to as a down-chirp signal because its frequency decreases rapidly. Like the process of finding $s_L^{(1)}(t)$, the LPF filter output in $\Delta T < t \leq 2\Delta T$ is calculated as

$$\begin{aligned} s_L^{(2)}(t) = \frac{1}{2}A_T \sum_{l=1}^{L} A_{R_l} \cos(2\pi((\frac{\Delta B}{\Delta T}t_{d_l} + f_{d_l})t \\ - (f_c + f_{d_l} + \frac{3\Delta B}{2})t_{d_l} - \frac{\Delta B}{2\Delta T}{t_{d_l}}^2)). \end{aligned} \tag{7}$$

Thus, if we apply the Fourier transform to (7), we can estimate the another beat frequency $\hat{f}_l^{(2)}$ of each cosine wave, which can be expressed as

$$\begin{aligned} \hat{f}_l^{(2)} &= \frac{\Delta B}{\Delta T}t_{d_l} + f_{d_l} \\ &= \frac{\Delta B}{\Delta T}\frac{2R_l}{c} + \frac{2v_l}{c}f_c. \end{aligned} \tag{8}$$

Therefore, if (5) and (8) are combined, R_l and v_l can be calculated as

$$R_l = (\hat{f}_l^{(1)} + \hat{f}_l^{(2)}) \times \frac{c\Delta T}{4\Delta B} \tag{9}$$

and

$$v_l = (\hat{f}_l^{(2)} - \hat{f}_l^{(2)}) \times \frac{c}{4f_c}. \tag{10}$$

However, if multiple targets exist simultaneously, it becomes difficult to pair the beat frequencies. In other word, ambiguity occurs in target range and velocity estimation. There are several methods to solve the beat frequency pairing problem [13], [20], [21]. Among several methods, we use a method that changes the time-frequency slope of the transmitted FMCW signal over time, as shown in Fig. 7. The transmitted signals in $2\Delta T < t \leq 4\Delta T$ and $4\Delta T < t \leq 6\Delta T$ also can be expressed as

$$s_t^{(3)}(t) = A_T \cos\left(2\pi(f_c - \frac{3\Delta B}{2})t + \pi\frac{\Delta B}{2\Delta T}t^2\right) \quad (2\Delta T \leq t \leq 4\Delta T) \tag{11}$$

and

$$s_t^{(4)}(t) = A_T \cos\left(2\pi(f_c + \frac{5\Delta B}{2})t - \pi\frac{\Delta B}{2\Delta T}t^2\right) \quad (4\Delta T \leq t \leq 6\Delta T). \tag{12}$$

Through the same process, the beat frequencies for each transmitted signal can be expressed as

$$\begin{aligned} \hat{f}_l^{(3)} &= \frac{\Delta B}{2\Delta T}t_{d_l} - f_{d_l} \\ &= \frac{\Delta B}{2\Delta T}\frac{2R_l}{c} - \frac{2v_l}{c}f_c \end{aligned} \tag{13}$$

and

$$\begin{aligned} \hat{f}_l^{(4)} &= \frac{\Delta B}{2\Delta T}t_{d_l} + f_{d_l} \\ &= \frac{\Delta B}{2\Delta T}\frac{2R_l}{c} + \frac{2v_l}{c}f_c. \end{aligned} \tag{14}$$

Therefore, if we use these four beat frequencies (e.g., $\hat{f}_l^{(1)}$, $\hat{f}_l^{(2)}$, $\hat{f}_l^{(3)}$, and $\hat{f}_l^{(4)}$), we can solve the target range and velocity ambiguity.

2) TARGET ANGLE ESTIMATION

For angle estimation, an array antenna system is used as a receiving antenna as described in Section II. Because the distance between the radar and the target is much larger than the spacing between the receiving antenna elements, we can consider the received radar signal as the far-field plane wave. Fig. 8 shows a conceptual diagram of an array antenna system. If we assume that the angle between the

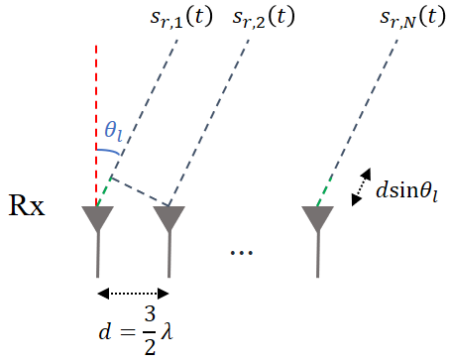

FIGURE 8. Array antenna system for angle estimation.

boresight direction of the array antenna and the l_{th} target is θ_l, the path difference between the signals received at each antenna element Δd can be calculated as $d \sin\theta_l$.

Therefore, the phase difference between the signal received from the first receiving antenna element $s_{r,1}(t)$ and the signal received from the n_{th} receiving antenna element $s_{r,n}(t)$ can be calculated as

$$\begin{aligned}\angle s_{r,n}(t) &= \angle s_{r,1}(t) + (n-1)\frac{2\pi}{\lambda} d\sin\theta_l \\ &= \phi_1 + (n-1)\Delta\phi,\end{aligned} \tag{15}$$

where ϕ_1 is the reference phase of the signal received from the first antenna element and $\Delta\phi$ is the phase difference of signals received from adjacent antenna elements. To estimate the angle θ_l of the l_{th} target, it is necessary to calculate $\Delta\phi$ because $\theta_l = \arcsin(\frac{\lambda}{2\pi d}\Delta\phi)$. Many estimation methods can be used to calculate the phase difference, such as the FFT, the Bartlett method, and the multiple signal classification (MUSIC) [22]. The performance of these algorithms is usually proportional to the number of array antenna elements N and the antenna spacing d.

In this work, we use the Bartlett method for the target angle estimation. In general, the angular resolution that can be obtained through the FFT in the N-element antenna system becomes $\frac{\lambda}{Nd\cos\theta}$ [23]. However, high-resolution angle estimation algorithms such as the Bartlett algorithm can overcome the limitations of the FFT-based angle estimation method [22]. The Bartlett method can be applied in real time due to the small amount of its computational load. In addition, it is robust to the change in the signal-to-noise ratio of the received signal compared to the subspace-based angle estimation methods, such as the estimation of signal parameters via rotational invariance techniques and the MUSIC [22]. Finally, the information of the l_{th} target, such as R_l, v_l, and θ_l, can be extracted using the aforementioned method.

B. SIGNAL PROCESSING FOR TARGET TRACKING

It is also important to track targets with detected target information. Therefore, we describe how to track the target with the target's distance, velocity, and angle information in this section. We first convert the target position given in the polar coordinate system to the 2D Cartesian coordinate system as follows:

$$\begin{aligned}z_l(k) &= \begin{bmatrix} x_l(k) \\ y_l(k) \end{bmatrix} \\ &= \begin{bmatrix} R_l(k)\sin\theta_l(k) \\ R_l(k)\cos\theta_l(k) \end{bmatrix},\end{aligned} \tag{16}$$

where k is the time index. With this converted position information, we apply the PDAF that can be used to track multiple radar targets. The tracking targets using the PDAF can be divided into four stages: the prediction, the measurement validation, the data association, and the state estimation. In the prediction stage, the state vector $\hat{x}(k|k-1)$, the measurement vector $\hat{z}(k|k-1)$, and the state covariance matrix $P(k|k-1)$ are predicted by applying the Kalman filter to those vectors and matrices of the previous time $k-1$. Here, we assume a constant velocity model when predicting the measurement vector $\hat{z}(k|k-1)$.

Then, in the measurement validation stage, it is determined whether the measured point $z(k)$ has entered a valid tracking area. The validation region $A(k)$ can be expressed as

$$\begin{aligned}A(k) = \{z(k) \,|\, &(z(k) - \hat{z}(k|k-1))^T \times S(k)^{-1} \\ &\times (z(k) - \hat{z}(k|k-1)) \le \gamma\},\end{aligned} \tag{17}$$

where γ and $S(k)$ are gate threshold corresponding to the gate probability P_γ and the innovation covariance matrix, respectively. According to (17), $z(k)$ follows the chi-squared distribution because the predicted measurement vector $\hat{z}(k|k-1)$ is the average value of $z(k)$ and the matrix $S(k)$ is the covariance matrix corresponding to the actual measurement. If the value of γ is determined, the value of P_γ is also determined, and vice versa. Thus, in this stage, we decide the radius γ for the data association.

Next, we calculate the association probability for each measured point in the gate threshold γ in the data association stage. Here, a nonparametric PDAF is used, which means that the probability of occurrence of all measured points in the radius γ is the same. Thus, the spatial density λ_P in the Poisson clutter model becomes $\frac{M(k)}{V(k)}$, where $M(K)$ and $V(K)$ denote the total number of measurement points in the gate threshold γ and the volume corresponding to the validation region $A(k)$. Then, the association probability to each measured point is calculated as

$$\beta_m(k) = \begin{cases} \dfrac{L_m(k)}{1 - P_\gamma P_D + \sum_{n=1}^{M(k)} L_n(k)} & (m = 1, 2, \cdots, M(k)) \\ \dfrac{1 - P_\gamma P_D}{1 - P_\gamma P_D + \sum_{n=1}^{M(k)} L_n(k)} & (m = 0), \end{cases} \tag{18}$$

where

$$\begin{aligned}L_m(k) = P_D \times \frac{V(k)}{M(k)} \times \frac{1}{2\pi|S(k)|^{1/2}} \exp(-\frac{1}{2}((z_m(k) \\ - \hat{z}(k|k-1))^T S(k)^{-1}(z_m(k) - \hat{z}(k|k-1))))\end{aligned} \tag{19}$$

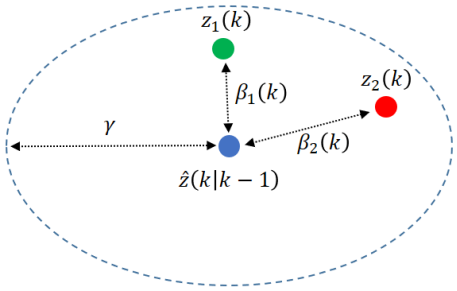

FIGURE 9. An example of the data association in the PDAF.

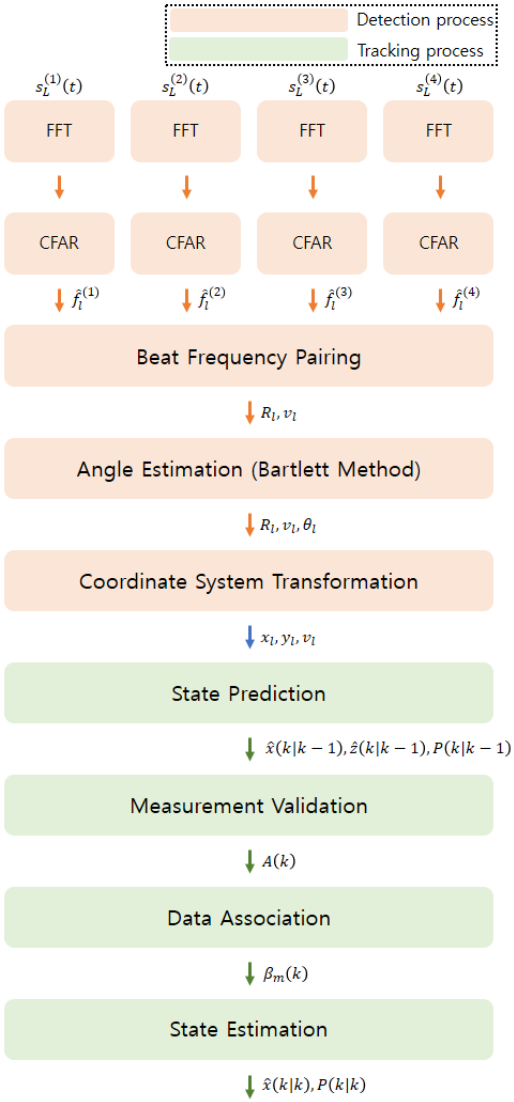

FIGURE 10. Overall signal processing chain of our traffic monitoring radar system.

and P_D is the probability of the target detection. For example, as shown in Fig. 9, we compute the association probability (e.g., $\beta_1(k)$ and $\beta_2(k)$) for measured points (e.g., $z_1(k)$ and $z_2(k)$) within the gate threshold γ.

Finally, using the calculated association probability, we update the state vector and the state covariance matrix from from $\hat{x}(k|k-1)$ and $P(k|k-1)$ to $\hat{x}(k|k)$ and $P(k|k)$. Therefore, the target can be tracked while performing this process every time k. The PDAF performs a nonlinear tracking because the association probabilities are calculated in a non-linear way, as shown in (18) and (19). Fig. 10 shows the overall signal processing flow diagram for target detection and tracking.

TABLE 2. Parameter values related to radar specifications.

Parameter	Value
Maximum detectable range (m)	300
Range resolution (m)	0.8
Detectable velocity range (km/h)	-250 ∼ 250
Velocity resolution (m/s)	1.2
Field of view (deg.)	-15 ∼ 15
Frame time (ms)	33

IV. MEASUREMENT RESULTS IN ACTUAL ROAD ENVIRONMENTS

A. MEASUREMENT ENVIRONMENTS

To verify the detection and tracking performance of our radar system, we installed the traffic monitoring radar on

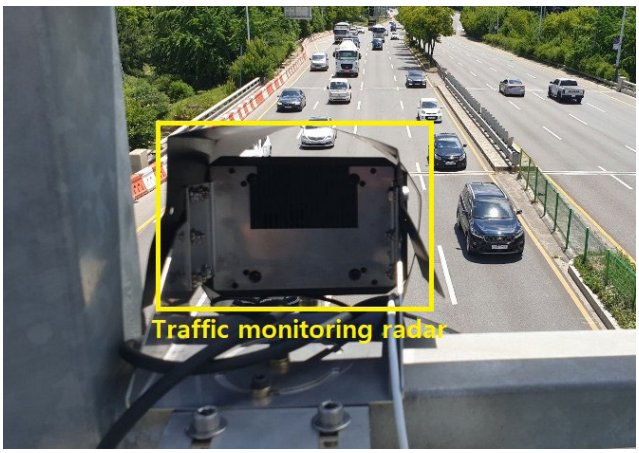

(a)

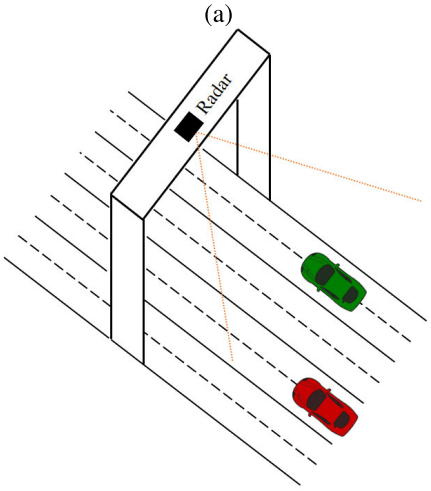

(b)

FIGURE 11. 24.1 GHz FMCW traffic monitoring radar installed on the pedestrian overpass: (a) a photograph (b) and a conceptual figure.

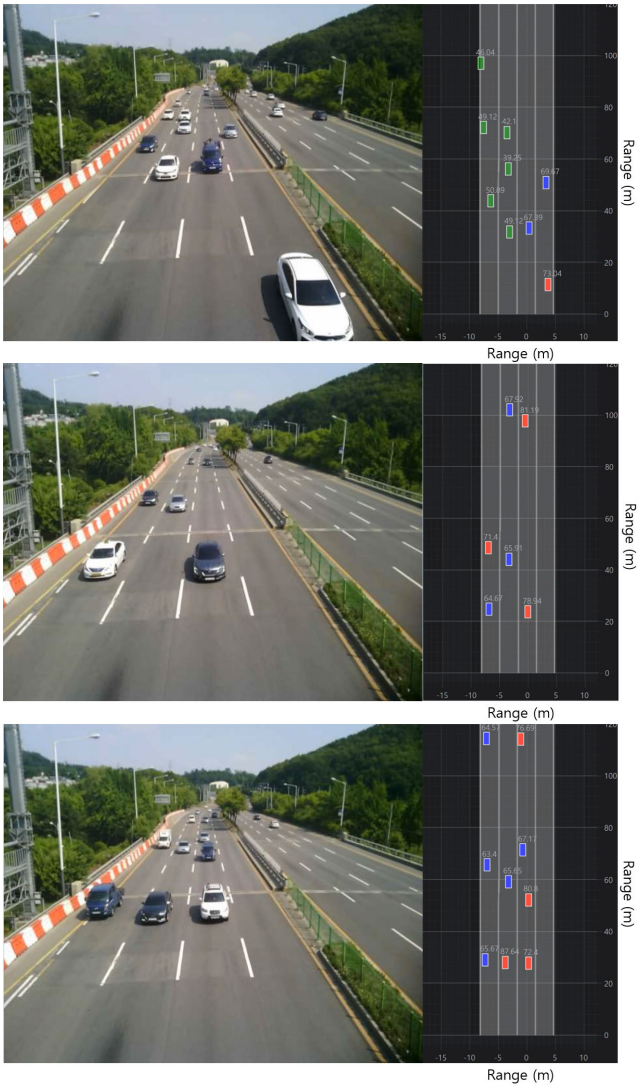

FIGURE 12. Actual measurement environments and target detection results.

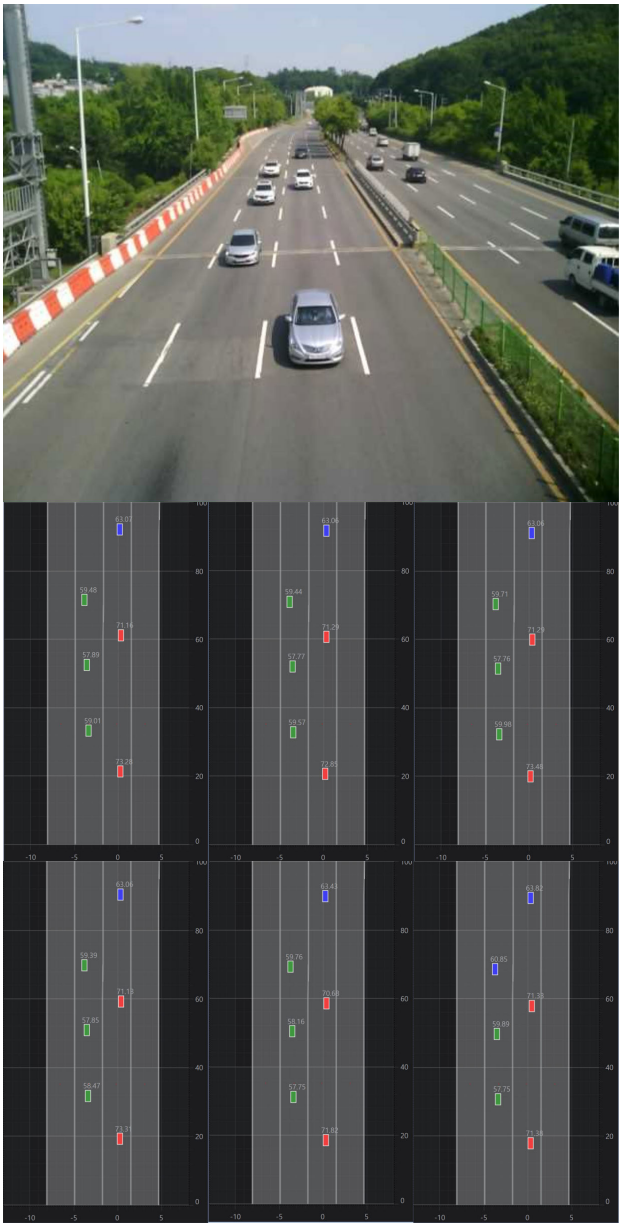

FIGURE 13. Actual measurement environments target tracking results for six consecutive frames.

the pedestrian overpass as shown in Fig. 11. Considering the antenna beam patterns of the transmit and receiving antennas given in Table 1, it was installed to cover the areas corresponding to the four lanes. Table 2 shows the parameter values related to the radar specifications determined from the FMCW radar waveform and the antenna system. The maximum detectable range can be derived from the radar equation [23] and the range resolution can be calculated from $\frac{c}{2\Delta B}$. In addition, the detectable velocity range and the velocity resolution are determined by the wavelength and sampling frequency [24]. The field of view of the radar is determined from the antenna beam patterns given in Fig. 2 and the antenna spacing.

B. TARGET DETECTION AND TRACKING RESULTS

Fig. 12 shows the detection results when the radar was installed on the overpass. Because the radar is fixed to the road structure, the relative distance and the relative velocity calculated from beat frequencies directly become the distance and the speed of the moving vehicles. When comparing the detection result on the right with the actual measurement environment on the left, the distances to several targets were well estimated. In the detection results on the right, the number displayed on the vehicle indicates the estimated velocity of each vehicle. In addition, we divided the velocity range that the radar can detect into several levels and displayed them in different colors in the figure. For example, green, blue, and, red represent speed ranges of 40∼60 km/h, 60∼70 km/h, and 70∼90 km/h, respectively. As shown in Fig. 12, our traffic monitoring radar can reliably estimate the distances and velocities of vehicles driving in all four lanes.

Moreover, Fig. 13 shows the tracking results for six vehicles driving in four lanes for six consecutive frames. As given in Table 2, because the time corresponding to one frame of

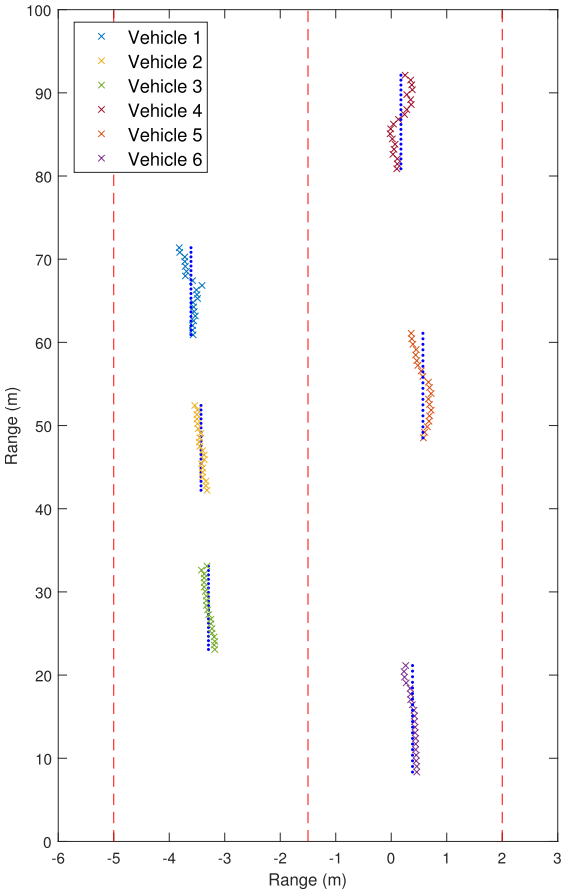

FIGURE 14. Actual and tracked trajectories for six vehicles.

the radar signal is 33 ms, the six frames are detection and tracking results corresponding to 0.2 s in total. As shown in the figure, the tracking algorithm with the PDAF reliably tracked multiple targets. Fig. 14 shows the actual and the tracked trajectories for the six targets. The reference trajectories of the vehicles were calculated by comparing the image obtained from the camera with the known road length. For the six vehicles, the root mean square error (RMSE) values of the tracked positions during the observation time was also calculated in Table 3. The RMSE value can be calculated as

$$RMSE = \sqrt{\frac{1}{K}\sum_{k=1}^{K}\left(p(k) - \hat{p}(k)\right)^2}, \tag{20}$$

where $p(k)$ and $\hat{p}(k)$ represent the reference and tracked position coordinates of the vehicle at time k. In addition, K denotes the number of frames. We can see that the targets are tracked without significant range errors because the PDAF is effective at tracking linearly moving objects. In the case of tracking using the PDAF, even if the target is missed two or three times, if the measured point $z_l(k)$ occurs in the predicted path, the missed target can be tracked again.

When two different vehicles intersect, the joint PDAF [25] and the multiple hypothesis testing [26] are more effective for the target tracking. However, these methods have a disadvantage in that they are difficult to apply in real time because the computational amount is much higher than that of the PDAF. Moreover, the intersection of the two vehicles on the highway means a traffic accident, and it does not occur often.

TABLE 3. RMSE values of the tracked positions for six vehicles.

Vehicle	RMSE value
Vehicle 1	0.126 (m)
Vehicle 2	0.085 (m)
Vehicle 3	0.117 (m)
Vehicle 4	0.142 (m)
Vehicle 5	0.133 (m)
Vehicle 6	0.082 (m)

V. CONCLUSION

In this article, we proposed a method to monitor road traffic with our own 24.1 GHz FMCW radar system. We first designed the transmit and receiving antenna system and the transceiver suitable for road traffic monitoring. Our radar system has a maximum detectable range of 300 m and a range resolution of 80 centimeters, so it can effectively detect vehicles in multiple lanes. Moreover, vehicles at the same distance can be sufficiently separated by angle information estimated using an array antenna system. To verify the detection and tracking performance of our radar, we installed it on the pedestrian overpass toward the highway. From the actual measurement results, it was confirmed that our radar system accurately estimated the positions and the velocities of vehicles moving in four lanes. In addition, the target tracking through PDAF was also achieved stably, and there was no significant difference between the actual target path and the tracked target path. When the traffic monitoring radars were installed over several overpasses, they showed stable detection and tracking performance. Road traffic monitoring using the radar system not only protects the privacy of a driver or a passenger, but also ensures robust detection and tracking performance even in climatic change. As a further study, we plan to conduct research to identify the type of vehicle by combining radar data with images acquired from cameras.

REFERENCES

[1] B. Maurin, O. Masoud, and N. P. Papanikolopoulos, "Tracking all traffic–computer vision algorithms for monitoring vehicles, individuals, and crowds," *IEEE Robot. Autom. Mag.*, vol. 12, no. 1, pp. 29–36, Mar. 2005.
[2] S. M. Patole, M. Torlak, D. Wang, and M. Ali, "Automotive radars: A review of signal processing techniques," *IEEE Signal Process. Mag.*, vol. 34, no. 2, pp. 22–35, Mar. 2017.
[3] S. Lee, B.-H. Lee, J.-E. Lee, and S.-C. Kim, "Statistical characteristic-based road structure recognition in automotive FMCW radar systems," *IEEE Trans. Intell. Transp. Syst.*, vol. 20, no. 7, pp. 2418–2429, Jul. 2019.
[4] M. Mercuri, P. J. Soh, G. Pandey, P. Karsmakers, G. A. E. Vandenbosch, P. Leroux, and D. Schreurs, "Analysis of an indoor biomedical radar-based system for health monitoring," *IEEE Trans. Microw. Theory Techn.*, vol. 61, no. 5, pp. 2061–2068, May 2013.
[5] S. Lim, S. Lee, J. Jung, and S.-C. Kim, "Detection and localization of people inside vehicle using impulse radio ultra-wideband radar sensor," *IEEE Sensors J.*, vol. 20, no. 7, pp. 3892–3901, Apr. 2020.
[6] P. Samczynski, K. Kulpa, M. Malanowski, P. Krysik, and L. Maslikowski, "A concept of GSM-based passive radar for vehicle traffic monitoring," in *Proc. Microw., Radar Remote Sens. Symp.*, Kiev, Ukraine, Aug. 2011, pp. 271–274.

[7] P. Krysik, K. Kulpa, M. Baczyk, L. Maslikowski, and P. Samczynski, "Ground moving vehicles velocity monitoring using a GSM based passive bistatic radar," in *Proc. IEEE CIE Int. Conf. Radar*, Chengdu, China, Oct. 2011, pp. 781–784.
[8] P. Gomez-Del-Hoyo, J. L. Barcena-Humanes, D. Mata-Moya, D. Juara-Casero, and V. Jimenez-de-Lucas, "Passive radars as low environmental impact solutions for smart cities traffic monitoring," in *Proc. IEEE EUROCON-Int. Conf. Comput. Tool (EUROCON)*, Salamanca, Spain, Sep. 2015, pp. 1–6.
[9] A. Riid, J. Kaugerand, J. Ehala, M. Jaanus, and J.-S. Preden, "An application of a low-cost microwave radar to traffic monitoring," in *Proc. 16th Biennial Baltic Electron. Conf. (BEC)*, Tallinn, Estonia, Oct. 2018, pp. 1–4.
[10] D. Felguera-Martin, J.-T. Gonzalez-Partida, P. Almorox-Gonzalez, and M. Burgos-García, "Vehicular traffic surveillance and road lane detection using radar interferometry," *IEEE Trans. Veh. Technol.*, vol. 61, no. 3, pp. 959–970, Mar. 2012.
[11] L. Cao, T. Wang, D. Wang, K. Du, Y. Liu, and C. Fu, "Lane determination of vehicles based on a novel clustering algorithm for intelligent traffic monitoring," *IEEE Access*, vol. 8, pp. 3892–3901, Mar. 2020.
[12] B. R. Mahafza, *Radar Systems Analysis and Design Using MATLAB*. Boca Raton, FL, USA: CRC Press, 2013.
[13] H. Rohling and M.-M. Meinecke, "Waveform design principles for automotive radar systems," in *Proc. CIE Int. Conf. Radar*, Beijing, China, Oct. 2001, pp. 1–4.
[14] Y. Bar-Shalom, F. Daum, and J. Huang, "The probabilistic data association filter," *IEEE Control Syst.*, vol. 29, no. 6, pp. 82–100, Dec. 2009.
[15] R. Behrendt, "*A priori* information to improve tracking for traffic monitoring," in *Proc. 16th Int. Radar Symp. (IRS)*, Dresden, Germany, Jun. 2015, pp. 1–6.
[16] R. Behrendt, "Traffic monitoring radar for road map calculation," in *Proc. 17th Int. Radar Symp. (IRS)*, Krakow, Poland, May 2016, pp. 1–4.
[17] F. B. Gross, *Smart Antennas for Wireless Communications With MATLAB*. New York, NY, USA: McGraw-Hill Professional, 2005.
[18] T. T. Taylor, "Design of line-source antennas for narrow beamwidth and low side lobes," *Trans. IRE Prof. Group Antennas Propag.*, vol. 3, no. 1, pp. 16–28, Jan. 1955.
[19] H. Rohling and R. Mende, "OS CFAR performance in a 77 GHz radar sensor for car application," in *Proc. Int. Radar Conf.*, Beijing, China, Oct. 1996, pp. 109–114.
[20] V. Winkler, "Range Doppler detection for automotive FMCW radars," in *Proc. Eur. Radar Conf.*, Munich, Germany, Oct. 2007, pp. 166–169.
[21] E. Hyun and J.-H. Lee, "A meothod for multi-target range and velocity detection in automotive FMCW radar," in *Proc. 12th Int. IEEE Conf. Intell. Transp. Syst.*, St. Louis, MO, USA, Oct. 2009, pp. 7–11.
[22] H. Krim and M. Viberg, "Two decades of array signal processing research: The parametric approach," *IEEE Signal Process. Mag.*, vol. 13, no. 4, pp. 67–94, Jul. 1996.
[23] S. Rao. *Introduction to mmwave Sensing: FMCW Radars*. Texas Instruments, Dallas, TX, USA. Accessed: Jan. 20, 2021. [Online]. Available: https://training.ti.com/sites/default/files/docs/mmwaveSensing-FMCW-offlineviewing_4.pdf
[24] J. Choi, "Interference mitigation scheme for automotive FMCW radar," Ph.D. dissertation, Dept. Elect. Comput. Eng., College Eng., Seoul Nat. Univ., Seoul, Republic of Korea, 2016.
[25] T. Fortmann, Y. Bar-Shalom, and M. Scheffe, "Sonar tracking of multiple targets using joint probabilistic data association," *IEEE J. Ocean. Eng.*, vol. 8, no. 3, pp. 173–184, Jul. 1983.
[26] S. S. Blackman, "Multiple hypothesis tracking for multiple target tracking," *IEEE Aerosp. Electron. Syst. Mag.*, vol. 19, no. 1, pp. 5–18, Jan. 2004.

HAE-SEUNG LIM received the B.S. and M.S. degrees in electronic engineering from Sogang University, Seoul, Republic of Korea, in 2010 and 2012, respectively, where he is currently pursuing the Ph.D. degree. From 2012 to 2019, he has worked as a Radar Signal Processing Engineer with the ADAS Division, Research and Development Center, Mando Corporation, Sungnam, Republic of Korea. His research interests include automotive radar system design, radar signal processing, and combining radar signal processing with machine learning algorithms.

HYUNG-MIN PARK (Senior Member, IEEE) received the B.S., M.S., and Ph.D. degrees in electrical engineering and computer science from the Korea Advanced Institute of Science and Technology (KAIST), Daejeon, South Korea, in 1997, 1999, and 2003, respectively. From 2003 to early 2005, he held a Postdoctoral position with the Department of Biosystems, KAIST. From 2005 to early 2007, he was with the Language Technologies Institute, Carnegie Mellon University. In 2007, he joined the Department of Electronic Engineering, Sogang University, Seoul, South Korea, where he is currently a Professor. His main research interests include multichannel speech processing and robust speech recognition.

JAE-EUN LEE received the B.S. and M.S. degrees in electronic and electrical engineering from the Pohang University of Science and Technology (POSTECH), South Korea, in 2006 and 2008, respectively, and the Ph.D. degree in electrical and computer engineering from Seoul National University, Seoul, South Korea, in 2017. He has started his career at Mando Corporation, after graduating from POSTECH, in 2008. He spent ten years at Mando as a Senior Researcher, where he registered 23 patents out of 80 filed patents to upgrade the RADAR solution and he also published ten journals world-wide during his stay at Mando. He is currently the CEO of Bitsensing Inc., and his goal is to redefine the safety to promote safer road environment through RADAR technology in the era of autonomous vehicles. Given his unique career in the field of RADAR, he was recognized by the Korean Government and was awarded as the Korean Engineer of the Year 2016 (also known as the 2016 IR52 Jang Youngshil Award).

YONG-HWA KIM (Member, IEEE) received the B.S. degree in electrical engineering and the Ph.D. degree in electrical and computer engineering from Seoul National University, Seoul, South Korea, in 2001 and 2007, respectively. From 2007 to 2011, he was a Senior Researcher with the Korea Electrotechnology Research Institute (KERI), South Korea. From 2011 to 2013, he was an Assistant Professor with the Division of Maritime Electronic and Communication Engineering, Mokpo National Maritime University, South Korea. In March 2013, he has joined the Faculty of the Department of Electronic Engineering, Myongji University, South Korea. His general research interests include communication systems, fault diagnosis, and digital signal processing. His particular research interests include artificial intelligence for communications, radar systems, and smart grid.

SEONGWOOK LEE (Member, IEEE) received the B.S. and Ph.D. degrees in electrical and computer engineering from Seoul National University (SNU), Seoul, Republic of Korea, in February 2013 and August 2018, respectively. From September 2018 to February 2020, he has worked as a Staff Researcher with the Machine Learning Laboratory, AI and SW Research Center, Samsung Advanced Institute of Technology (SAIT), Suwon, Republic of Korea. Since March 2020, he has been an Assistant Professor with the School of Electronics and Information Engineering, College of Engineering, Korea Aerospace University, Goyang, Republic of Korea. He has published more than 50 articles on radar signal processing. His research interests include automotive radar signal processing techniques, such as improved angle estimation, target recognition and classification, clutter suppression, mutual interference mitigation, and target tracking. He received the Distinguished Ph.D. Dissertation Award from the Department of Electrical and Computer Engineering, SNU.